

Automatic Recognition of the Hepatocellular Carcinoma from Ultrasound Images using Complex Textural Microstructure Co-Occurrence Matrices (CTMCM)

Delia Mitrea¹, Sergiu Nedevschi¹ and Radu Badea²

¹Computer Science Department, Technical University of Cluj-Napoca, Baritiu Str., No. 26-28, Cluj-Napoca, Romania

²I. Hatieganu University of Medicine and Pharmacy, V. Babes Str., No. 8, Cluj-Napoca, Romania

Keywords: Complex Textural Microstructure Co-occurrence Matrices (CTMCM), Textural Model, Hepatocellular Carcinoma, Ultrasound Images, Classification Performance.

Abstract: The hepatocellular carcinoma is one of the most frequent malignant liver tumours. The golden standard for HCC detection is the needle biopsy, but this is a dangerous technique. We aim to perform the non-invasive recognition of this tumour, using computerized methods within ultrasound images. For this purpose, we defined the textural model of HCC, consisting of the relevant textural features that separate this tumour from other visually similar tissues and of the specific values that correspond to these relevant features: arithmetic mean, standard deviation, probability distribution. In this paper, we demonstrate the role that the Complex Textural Microstructure Co-occurrence Matrices have in the improvement of the textural model of HCC and in the increase of the recognition performance. During the experiments, we considered the following classes: cirrhosis, HCC, cirrhotic parenchyma on which HCC evolved and hemangioma, a frequent benign liver tumour. The resulted recognition accuracy for HCC was towards 90%.

1 INTRODUCTION

The hepatocellular carcinoma (HCC) is the most frequent malignant liver tumour, occurring in 70% of the liver cancer cases. It evolves from cirrhosis, after a phase of liver parenchyma restructuring at the end of which dysplastic nodules (future malignant tumours) result (American Liver Foundation, 2015). The most reliable method for HCC diagnosis is the needle biopsy, but this technique is invasive, dangerous, as it could lead to the spread of the tumour inside the human body. We develop non-invasive, computerized methods for the automatic and computer assisted diagnosis of this tumour, based on ultrasound images. Ultrasonography is a reliable method for patient examination and monitoring, being safe, non-invasive, inexpensive and repeatable. Other examination techniques that involve medical imaging, such as the computer tomography, the magnetic resonance imaging, the endoscopy, even the contrast enhanced ultrasonography or elastography, are irradiating and/or expensive. Concerning the aspect of the HCC tumour in ultrasound images, in incipient phase, it

appears as a small lesion (2-3 cm), usually having a hypoechogenic and homogeneous aspect. In more advanced phases, mostly often, its aspect becomes hyperechogenic and heterogeneous, due to the interleaving of many tissue types (fibrosis, necrosis, active growth tissue, fatty cells) and to the complex vessel structure (Sherman, 2005). However, it is difficult to distinguish this tumour from the surrounding cirrhotic parenchyma, and also it sometimes resembles the benign tumours. Texture is an important property in this context, being able to reveal subtle characteristics of the tissue, beyond the perception of the human eye. In nowadays' research, there are many approaches involving the combination between the texture analysis methods and various classifiers, aiming to perform the recognition of some severe pathologies, based on ultrasound images (Sujana et al., 1996), (Yoshida et al., 2003), (Madabhushi, 2005), (Chikui, 2005), (Duda et al., 2013), (Masood, 2006). In our former research, we defined the textural model of HCC, consisting of the complete set of relevant textural features that best characterize this tumour, respectively of the specific values associated to the

relevant textural features: mean, standard deviation and probability distribution. For texture analysis, we previously employed classical methods, such as the first order statistics of the grey levels (arithmetic mean, maximum and minimum values), the autocorrelation index, the grey level co-occurrence matrix of order two and the associated Haralick features, edge-based statistics, the frequency of the textural microstructures derived by using the Laws' convolution filters, the Hurst fractal index, the Shannon entropy computed after applying the Wavelet transform at two resolution levels (Meyer-Base, 2009). We also developed more accurate texture analysis techniques, such as the GLCM matrix of superior order (Mitrea, D., et al., 2012), (Mitrea, D., Mitrea, P. et al., 2012), the edge orientation co-occurrence matrix of second and third order (Mitrea, D., Mitrea, P. et al., 2012), respectively the Textural Microstructure Co-occurrence Matrices (TMCM) of second and third order, all these techniques being experimented in the context of abdominal tumour recognition based on ultrasound images (Mitrea et al., 2014). In this work, we highlighted the role that our newly defined Complex Textural Microstructure Co-occurrence Matrices (CTMCM) of order two and three, which involved a set of Laws' features, as well as gradient features, had in the supervised recognition of the HCC tumour.

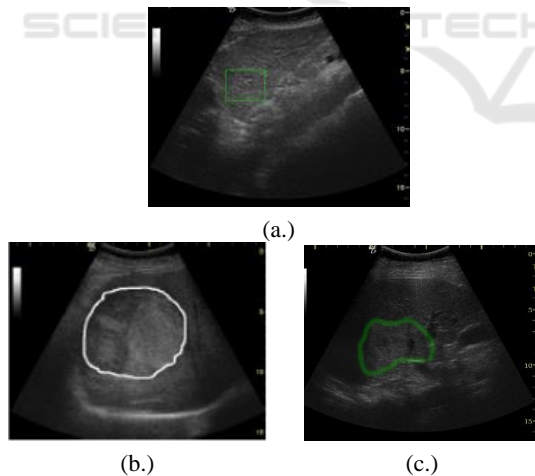


Figure 1: Representative US images for (a.) Cirrhosis; (b.) HCC; (c.) Hemangioma.

The Laws' based CTMC was experimented before in the context of the liver tumour recognition, in the unsupervised detection of the HCC evolution phases (Mitrea et al., 2016), and also for colo-rectal tumour recognition, providing satisfying results (Mitrea et al., 2015). In this paper, we compare the

role that the CTMCM based on Laws' textural microstructures, or gradient features, have in increasing the supervised recognition accuracy of the HCC tumour and liver cancer.

We assessed the improvement of the textural model and the classification performance increase by providing the new set of relevant textural features at the inputs of some powerful classifiers and meta-classifiers such as: Support Vector Machines (SVM), Multilayer Perceptron (MLP), decision trees (C4.5), AdaBoost combined with C4.5. We compared the performance due to the newly defined textural features with that provided by the formerly existing textural features. The experimental dataset consisted of B-mode ultrasound images representing liver tissue affected by cirrhosis, hepatocellular carcinoma, cirrhotic parenchyma surrounding the HCC tumour, and also the hemangioma benign tumour. Relevant images belonging to each of these classes are illustrated in Figure 1. When taking into account the newly defined textural features, the obtained accuracy for HCC recognition was towards 90%.

2 THE STATE OF THE ART

The texture-based methods were widely used during nowadays' research, in combination with classifiers, with the purpose of the automatic recognition of the tumours within medical images (Yoshida et al., 2003), (Madabhushi, 2005), (Chikui, 2005), (Duda et al., 2013), (Masood, 2006). Thus, methods like the Wavelet and Gabor transforms were used in combination with Artificial Neural Networks (ANN) and Bayesian classifiers for the recognition of the liver and prostate tumours from ultrasound (Sujana et al., 1996), (Yoshida et al., 2003) and magnetic resonance (MRI) images (Madabhushi, 2005), the fractal-based methods were used for the recognition of the salivary gland tumours in (Chikui, 2005), while the run-length matrix parameters, in combination with the Haralick features derived from the GLCM matrix were used in conjunction with ANN classifiers, Support Vector Machines and Fisher Linear Discriminants, for the automatic recognition of the liver lesions (Sujana et al., 1996). In a more recent approach, the authors performed the recognition of the liver tumours based on the computation of the textural parameters from typical and contrast enhanced computer tomographic (CT) images. Feature selection was performed and then a C4.5 classifier was applied, which provided a recognition rate above 90% (Duda et al., 2013).

The technique of Grey Level Co-occurrence Matrix (GLCM) was frequently used with the purpose of tumour characterization and recognition within ultrasound images and proved its efficiency in many situations. A representative approach is described in (Khuzir et al., 2009), where the GLCM method was implemented in conjunction with a decision trees based classifier, in order to perform the recognition of the breast lesions from mammographic images. This matrix was computed for the following directions: 0° , 45° , 90° , 135° and the corresponding Haralick features were derived. The accuracy, measured in terms of the area under the ROC curve, was 84%. The generalized co-occurrence matrices, defined by Davis (Davis, 1979), were recently used in the form of the Local Binary Pattern (LBP) Co-occurrence Matrix (Sujatha et al., 2012), respectively in the form of the texton and texture orientation co-occurrence matrix (Sujatha et al., 2013). In the context of the research described in (Sujatha et al., 2012), the authors firstly performed texton detection, by applying specific convolution filters, then the Local Binary Pattern (LBP) method was applied; the logically compact LBP features were also determined, after applying the OR operator among the neighbours of the current pixel. At the end, the Logical Compact Local Binary Pattern Co-occurrence Matrix (LCLBPM) was determined and experimented on standard textures from the VisTex database, providing a satisfying classification accuracy, situated between 80%-98%, better than that provided by the Gabor features applied in the same context. In the work described in (Sujatha et al., 2013), the authors applied convolution filters for texton detection, then they determined the texton co-occurrence matrix for the following directions of the displacement vectors: 0° , 45° , 90° , 135° . The texture orientation co-occurrence matrix was also determined, after computing the orientation of the edges resulted after the application of the Sobel and Canny specific methods. These methods were experimented on the VisTex database and provided recognition rates situated between 89% - 98.8%. As it results from the above-described approaches, there does not exist any significant study involving a co-occurrence matrix based on textural microstructures determined after applying the Laws' convolution filters, or multiple edge detection filters. Also, there is no systematic study of the relevant textural features that best characterize HCC, in the context of the automatic recognition of this tumour. In our previous research, we defined the textural model of the malignant tumours (Mitrea et al., 2012), useful in both automatic and computer

aided diagnosis. In this work, we analyse the efficiency of the Complex Textural Microstructure Co-occurrence Matrices (CTMCM) in the context of HCC recognition from ultrasound images.

3 THE PROPOSED SOLUTION

3.1 The Imagistic Textural Model of the Hepatocellular Carcinoma

The imagistic textural model of the hepatocellular carcinoma (HCC), also defined in (Mitrea et al., 2012), consists of:

- The complete set of the relevant textural features able to differentiate this tumour from visually similar classes
- The specific values associated to the relevant textural features: arithmetic mean, standard deviation, probability distribution.

In order to build the imagistic textural model, the following phases are necessary: first, a preliminary phase is performed, when the training set is built, consisting of regions of interest selected inside the tissue of interest, within the ultrasound images. Then, an image analysis phase is due, when the textural features are computed by applying specific, texture analysis methods. The learning phase consists of selecting the relevant textural features, respectively of computing the specific values of the relevant textural features (arithmetic mean, standard deviation, probability distribution). At the end, the validation phase is performed, when the values of the relevant textural features are provided to classifier inputs and supervised classification methods are applied in order to assess the classification performance due to the generated imagistic textural model.

3.2 The Image Analysis Phase

During the image analysis phase, classical textural features, as well as newly defined textural features, derived from advanced texture analysis methods, were computed. Thus, first order statistics of the grey levels (the arithmetic mean, the standard deviation and the probability distribution), edge-based statistics (the edge frequency, edge contrast, the average edge orientation), the density and frequency of the textural microstructures obtained after applying the Laws convolution filters, second order statistics of the grey levels (the autocorrelation index, the Gray Level Co-occurrence Matrix -

GLCM of order two), the Hurst fractal index, as well as the Shannon entropy computed after applying the Wavelet transform, recursively, twice, were determined in the first phase. Then, the GLCM of order 3, 5 and 7, as well as the Edge Orientation Co-occurrence Matrix (EOCM) of order 2 and 3 and the associated Haralick features were also computed. In addition, a new type of superior order generalized co-occurrence matrix, the Complex Textural Microstructure Co-occurrence Matrix (CTMCM) of order two and three was employed and analysed in the current work, as described below.

3.2.1 The Complex Textural Microstructure Co-Occurrence Matrix (CTMCM) of Second and Superior Order

The Complex Textural Microstructure Co-occurrence Matrix (CTMCM) was determined through the methodology described below, consisting of the following steps:

- (1) First, we associated feature vectors to the pixels in the region of interest, consisting of:
 - the results obtained after applying the 2D Laws' convolution filters for detecting levels, edges, spots, waves, ripples and also combined microstructures (L5L5, E5E5, S5S5, W5W5, R5R5, S5R5, R5S5), in the case of the Laws' based CTMCM (Laws, 1980).
 - the results obtained after applying edge detection filters: the Sobel filters for identifying horizontal and vertical edges (Meyer-Base, 2009), the Kirsch Compass filters for finding edges with different orientations (Kirsch, 1971), as well as the Laplacian convolution filter, in the case of the edge-based CTMCM (Meyer-Base, 2009).
- (2) Then, we applied an improved k -means clustering method, in the following manner: we started from a minimum number of centres ($k=50$); this number was increased by splitting the corresponding centres; a centre was split in two other centres, if the standard deviation of the items within the corresponding class (cluster) overpassed the threshold equal with $\frac{3}{4}$ of the average standard deviation of all the existing classes. The newly resulted centres were computed as being $\frac{1}{2}$ of the old centre, respectively $\frac{3}{2}$ of the old centre.
- (3) All the labels of the pixels from the region of interest (ROI) were re-assigned after splitting the old centres, then the step (2) was performed again. The condition for the algorithm to finish was the convergence, the maximum number of centres being also established to 200. The solution of the algorithm (the optimal solution) corresponded to the

minimum value of WCSS (Within Cluster Sum of Squared Errors) (Duda, 2003). Thus, the definition of the Complex Textural Microstructure Co-occurrence Matrix (CTMCM) was provided in (1):

$$\begin{aligned}
 C_D(t_1, t_2, \dots, t_n) &= \#\{(x_1, y_1), (x_2, y_2), (x_3, y_3), \dots, (x_n, y_n)\}: \\
 A(x_1, y_1) &= t_1, A(x_2, y_2) = t_2, \dots, A(x_n, y_n) = t_n, \\
 |x_2 - x_1| &= |\vec{d}x_1|, |x_3 - x_1| = |\vec{d}x_2|, \dots, |x_n - x_1| = |\vec{d}x_{n-1}|, \\
 |y_2 - y_1| &= |\vec{d}y_1|, |y_3 - y_1| = |\vec{d}y_2|, \dots, |y_n - y_1| = |\vec{d}y_{n-1}|, \\
 \text{sgn}((x_2 - x_1)(y_2 - y_1)) &= \text{sgn}(\vec{d}x_1 \cdot \vec{d}y_1), \dots \\
 \text{sgn}((x_n - x_1)(y_n - y_1)) &= \text{sgn}(\vec{d}x_{n-1} \cdot \vec{d}y_{n-1})
 \end{aligned} \tag{1}$$

In (1), the # symbol represents the number of elements of the set specified between the braces and

$$\vec{d} = ((\vec{d}x_1, \vec{d}y_1), (\vec{d}x_2, \vec{d}y_2), \dots, (\vec{d}x_{n-1}, \vec{d}y_{n-1})) \tag{2}$$

are the displacement vectors. „A” stands for the attribute associated to each pixel, while t_1, t_2, \dots, t_n are the values of the textons (cluster labels) obtained after the application of the improved k -means clustering algorithm. Thus, each element of the CTMCM matrix represents the number of the n -tuples of pixels, with the coordinates $(x_1, y_1), (x_2, y_2), \dots, (x_n, y_n)$ having the cluster labels t_1, t_2, \dots, t_n and being in a spatial relationship defined by the displacement vectors. We computed the CTMCM matrix of order two and three and we determined the corresponding Haralick parameters, in a similar way as described in (Mitrea et al., 2015). For the CTMCM of order two, the following directions were considered: $0^\circ, 90^\circ, 180^\circ$, and 270° . For the CTMCM of order three, the current pixel was considered in the central position and together with the other two pixels, they were either collinear, or formed a right angle triangle (the current pixel being in the position of the right angle). We considered the following orientations for the two displacement vectors: $(0^\circ, 180^\circ), (90^\circ, 270^\circ), (45^\circ, 225^\circ), (135^\circ, 315^\circ)$ for the case of collinear pixels; $(0^\circ, 90^\circ), (90^\circ, 180^\circ), (180^\circ, 270^\circ), (0^\circ, 270^\circ), (45^\circ, 135^\circ), (135^\circ, 225^\circ), (225^\circ, 315^\circ), (45^\circ, 315^\circ)$, for the right angle triangle case. The displacement vectors had the absolute value 2, in both cases. We determined the CTMCM matrices for all the considered direction combinations of the displacement vectors, the final features resulting as an average between the Haralick features of the individual matrices, just as in the case of the superior order GLCM, respectively EOCM. We also extended the cluster shade and cluster prominence features at order n , and we computed the maximum area of the intersection of the corresponding histogram with a horizontal plane,

as described in (Mitrea et al., 2016); (Nanni et al., 2013).

3.3 The Learning Phase

3.3.1 Feature Selection Methods

In order to derive the set of the relevant textural features, the following methods were considered, which provided the best results in our former experiments: Correlation based Feature Selection (CFS) combined with genetic search, respectively Gain Ratio Attribute Evaluation combined with the Ranker method. The method of Correlation-based Feature Selection (CFS) assigned a merit to each group of features with respect to the class parameter (Hall, 2003), as described by the formula (3). In (3)

$\overline{r_{cf}}$ represents the average correlation of the features to the class, $\overline{r_{ff}}$ is the average correlation between the features, while k is the number of the elements in the subset.

$$Merit_s = \frac{k\overline{r_{cf}}}{\sqrt{k + k(k-1)\overline{r_{ff}}}} \quad (3)$$

The second technique assessed the individual features by assigning them a gain ratio with respect to the class (Hall, 2003), as provided in (4). In (4), $H(C)$ is the entropy of the class parameter, $H(C|A_i)$ is the entropy of the class after observing the attribute A_i , while $H(A_i)$ is the entropy of the attribute A_i .

$$GainR(A_i) = (H(C) - H(C|A_i)) / H(A_i) \quad (4)$$

The final relevance score for each feature was obtained by computing the arithmetic mean of the individual relevance values provided by each method. Only those features that had a significant value for the final relevance score (above a threshold) were taken into account.

3.3.2 The Specific Values for the Relevant Textural Features

The specific values of the relevant textural features (the arithmetic mean, the standard deviation, respectively the probability distribution) were computed using the Weka library (Weka, 2017). In order to determine the probability distribution for each feature, with respect to the class, the method of

Bayesian Belief Networks (Duda, 2003) was adopted. The technique of Bayesian Belief Networks detects influences between the features, by generating a dependency network, which is represented as a directed, acyclic graph (DAG). In this graph, the nodes represent the features, while the edges stand for the causal influences between these features, having associated the values of the corresponding conditional probabilities. Every node X in this graph has a set of parents, P and a set of children, C . Within a Bayesian Belief Network, each node has associated a probability distribution table, indicating the specific intervals of values for that node, given the values of its parents.

3.3.3 Textural Model Assessment through Supervised Classification

The following supervised classifiers and classifier combinations, well known for their performance, which provided the best results in the context of our experiments, were taken into account: the Multilayer Perceptron (MLP), the Support Vector Machines (SVM), the Random Forest (RF) classifier, as well as the AdaBoost meta-classifier combined with the C4.5 method for decision trees. For the Multilayer Perceptron, multiple architectures were experimented and the best one was adopted in each case. For classification performance assessment, we considered the following parameters: the classification accuracy (recognition rate), the TP rate (sensitivity), the TN rate (specificity), as well as the area under the ROC curve (AUC) (Duda, 2003).

4 EXPERIMENTS AND DISCUSSIONS

For the experiments, we used 100 cases of cirrhosis, 300 cases of HCC, together with the cirrhotic parenchyma on which HCC had evolved, respectively 100 cases of hemangioma. All these patients underwent biopsy, for diagnostic confirmation. For each patient, 3 images were considered, for various orientations of the transducer. The images were acquired by our research collaborators, the medical specialists from the 3rd Medical Clinic of Cluj-Napoca, using a Logiq 7 ultrasound machine, at the same settings: frequency of 5.5 MHz, the gain of 78 and the depth of 16 cm. On each image, a region of interest, having 50x50 pixels in size, was selected manually inside the corresponding class of tissue, this process being supervised by the medical specialists in

radiology. A number of 90 textural features were computed on each ROI independently on orientation, illumination and region of interest size, using our Visual C++ software modules. The values of the textural features followed by the class specification represented an instance of the training set. In the context of binary classification, the classes were combined in equal proportion inside the training set (the two considered classes always had the same number of instances). The feature selection methods and the classification techniques were implemented on the dataset using the Weka library (Weka3, 2017). For feature selection, we used Correlation based Feature Selection (CFS) in combination with genetic search, respectively Gain Ratio Attribute Evaluation in combination with the ranker method, as all these techniques provided the best results in our experiments. For classification, we used the following algorithms of the Weka library: John Platt's Sequential Minimal Optimization (SMO) for implementing SVM; in this case, we used one of the second or third degree polynomial kernels, the input data being normalized. The J48 method, standing for the C4.5 algorithm, was adopted as well; also, the AdaBoost meta-classifier with 100 iterations, in conjunction with the J48 method was employed. For the RF method, we used the Weka's algorithm with the same name, with 100 trees. The MultilayerPerceptron (MLP) classifier was also adopted. Multiple architectures of this classifier were experimented, in the following manner: the total number of nodes was always equal with the arithmetic mean between the number of attributes and the number of classes $(no_of_attributes+no_of_classes)/2$, while the number of layers was one, two or three, the nodes being equally distributed among the layers. For the MLP classifier, the learning rate was 0.2 and the value of α parameter was fixed to 0.8, in order to achieve both high speed and high accuracy for the learning process (Weka, 2017). After all the parameters of these classifiers were assigned, the strategy of cross-validation with 5 folds was implemented on the dataset, for classification performance assessment, using the Weka library.

4.1 The Role of the CTMCM Matrices in the Differentiation between Cirrhosis and Cirrhotic Parenchyma around HCC

- The relevant textural features derived from the Laws' based CTMCM matrix

The set of the textural features which were relevant concerning the differentiation between cirrhosis and the cirrhotic parenchyma on which HCC had evolved are provided in (5):

$$\{Laws_CTMCM3_Energy, Laws_CTMCM3_Entropy, Laws_CTMCM_Entropy, Laws_CTMCM_Homogeneity, Laws_CTMCM3_MaxArea, Wavelet_Entropy1, Wavelet_Entropy4, Laws_CTMCM_Correlation, Laws_CTMCM3_ClusterProminence, Laws_CTMCM3_Homogeneity, Wavelet_Entropy5_hl, Wavelet_Entropy5_ll, Wavelet_Entropy5_lh, Wavelet_Entropy5_hh, Wavelet_Entropy6_ll, Wavelet_Entropy6_hl, Wavelet_Entropy6_hh, Wavelet_Entropy6_lh, Wavelet_Entropy2, Wavelet_Entropy3, Min_Grey_Level, GLCM_Contrast, Edge_Orientation_Variability, Directional_Grad_Variability, Laws_CTMCM_ClShade, Laws_Spot_Frequency, Laws_CTMCM_ClProminence, Laws_Spot_Mean, Laws_CTMCM3_ClusterShade\} \quad (5)$$

We can notice the importance of the textural features derived from the second and third order Laws' based CTMCM matrix. Most of these features were situated on the first seven positions within the feature ranking. From this set, the second and third order CTMCM Energy, the second order CTMCM Entropy, as well as the second order CTMCM Homogeneity denoted differences in homogeneity between liver cirrhosis and the cirrhotic parenchyma which surrounds HCC and also the more accentuated chaotic character of the cirrhotic parenchyma structure, due to a more evolved restructuring process. The CTMCM maximum area parameter emphasizes the more increased structural complexity of the cirrhotic parenchyma on which HCC had evolved, in comparison with cirrhosis. We can also notice the relevance of the second and third order CTMCM Cluster Prominence parameter and of the third order CTMCM Cluster Shade feature. Another important relevant feature was the CTMCM Correlation, denoting differences in granularity between the two considered classes, due to the evolving restructuring process. While the features derived from the CTMCM matrices together with the Laws Spot Mean and with the Laws Spot Frequency express differences in homogeneity, structural complexity and granularity in terms of textural microstructures, the other relevant textural features, derived from the GLCM matrix or referring to edge-based statistics, emphasize these differences in terms of grey levels or edges. The entropy

computed at multiple levels, after applying the Wavelet transform twice, is also present at a great extent among the relevant features, expressing the fact that the increasing chaotic character of the tissue structure, which is due to the restructuring process, can be visualized at multiple resolutions.

- **The relevant textural features derived from the edge based CTMCM matrix**

In order to assess the role of the edge based CTMCM matrix in the differentiation between cirrhosis and the cirrhotic parenchyma on which HCC had evolved, we considered the set formed by the previously existing textural features, respectively edge based CTMCM features. The relevant textural features resulted after applying the feature selection methods described in 3.3.1 are depicted in (6).

$$\{ \text{Edge_CTMCM_Max_Area, Wavelet_Entropy4, Edge_CTMCM3_Max_Area, Min_Grey_Level, Edge_CTMCM_Entropy, Wavelet_Entropy1, Wavelet_entropy5_lh, Wavelet_Entropy5_hl, Wavelet_Entropy5_hh, Wavelet_entropy5_ll, Wavelet_Entropy6_hh, Wavelet_Entropy6_ll, Wavelet_Entropy6_hl, Wavelet_Entropy2, Edge_CTMCM3_Entropy, Edge_CTMCM_Homogeneity, GLCM_Contrast, Edge_Contrast, GLCM_Variance, Wavelet_Entropy_3, Edge_CTMCM_Energy, Directional_gradient_variability, Laws_Spot_Frequency, Laws_Spot_Mean, Laws_Ripple_Mean} \} \quad (6)$$

From (6), it results the importance of the newly defined features Maximum Area derived from the second and third order edge based CTMCM matrix, denoting differences in structural complexity between the two considered classes (cirrhosis and cirrhotic parenchyma on which HCC had evolved). The entropy derived from the second and third order CTMCM matrix, as well as the homogeneity computed from the CTMCM matrix of order two are also met among the relevant textural features, emphasizing, in terms of edges, differences in homogeneity between the liver affected by cirrhosis and the cirrhotic parenchyma on which HCC had evolved. The other part of the set containing the relevant textural features, illustrated in (6), has an extended intersection with the relevant textural feature set described in (5), the entropy computed on various components resulted after applying the

Wavelet transform at multiple resolutions being met in this case as well.

- **Class differentiation accuracy, due to the CTMCM matrices**

Figure 2 illustrates the comparison among the classification accuracies resulted when considering various CTMCM features in combination with the already existing (old) textural features. The following feature sets were taken into account: the old textural features, including classical textural features, superior order GLCM features and EOCM features; the old textural features combined with the edge-based CTMCM features; the old textural features combined with the Laws' based CTMCM features. Thus, we notice that the feature sets including the newly defined textural features, derived from the Laws' based CTMCM matrix and from the edge-based CTMCM matrix led to an increase in accuracy, for each considered classifier, in comparison with the set containing only the old textural features. The highest recognition rate, of 86.71%, resulted in the case of the AdaBoost meta-classifier combined with the J48 method (AdaBoost+J48), when considering the set containing the old textural features combined with the edge based CTMCM features. In this case, the best structure of the MLP classifier, that provided the highest values for the performance parameters, consisted of three layers.

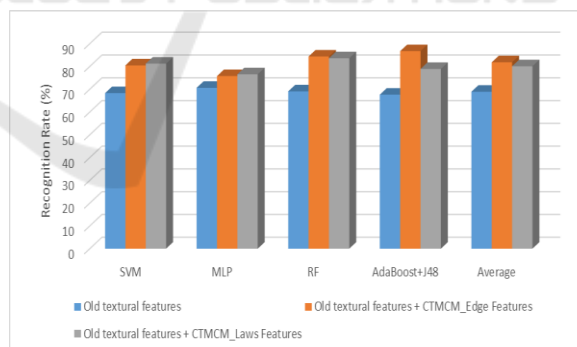


Figure 2: The increase in accuracy due to the newly defined textural features when differentiating between cirrhosis and cirrhotic parenchyma on which HCC had evolved.

Concerning the arithmetic mean of the recognition rates, for all the classifiers, in the case of each textural feature set, the highest mean value, of 81.83%, resulted for the set containing the old textural features combined with the edge based CTMCM features, followed by that resulted when combining the Laws' based CTMCM features with

the old textural features (80.075%), and then by the mean accuracy value which corresponded to the old textural feature set (68.89%). Concerning the other classification performance parameters, the highest sensitivity (TP Rate) of 87.8% and the highest AUC of 88.2%, resulted in the case of the AdaBoost meta-classifier combined with the J48 technique, while the highest specificity (TP Rate) of 85.2% resulted in the case of the SMO classifier.

4.2 The Role of the CTMCM Matrices in the Differentiation between HCC and the Cirrhotic Parenchyma around HCC

- **The relevant textural features derived from the Laws' based CTMCM matrix**

The relevant textural features obtained in this case, when considering the set formed by the previously existing textural features and the Laws' based CTMCM features, are illustrated in (7).

{EOCM3_Energy, EOCM3_Entropy, GLCM7_entropy, Laws_CTMCM3_Contrast, Laws_CTMCM_Contrast, Laws_CTMCM_Correlation, GLCM5_Entropy, EOCM3_Correlation, GLCM3_Energy, GLCM7_Energy, Wavelet_Entropy4, EOCM3_Contrast, EOCM3_Variance, Laws_CTMCM_Variance, Laws_CTMCM3_Variance, Wavelet_Entropy6_lh, Wavelet_Entropy6_hl, Wavelet_Entropy6_ll, Wavelet_entropy6_hh, Wavelet_entropy5_ll, Wavelet_entropy5_lh, Wavelet_entropy5_hh, Wavelet_Entropy1, Wavelet_Entropy2, Wavelet_Entropy3, EOCM_Variance, GLCM7_Correlation, GLCM7_Variance, Min_grey_level, Laws_CTMCM_Homogeneity, GLCM_Variance}

(7)

We remark that the contrast derived from the second and third order CTMCM matrices, as well as the correlation derived from the second order CTMCM matrix are situated on the top of the relevant feature ranking in this case. The variance derived from the second and third order CTMCM and the homogeneity computed from the second order CTMCM are relevant as well. These features emphasize the complex structure of the tumour tissue (the contrast and the variance computed from

the second and third order CTMCM), the differences in granularity which exist between HCC and the cirrhotic parenchyma on which HCC had evolved (the CTMCM Correlation) and also the heterogeneous structure of the HCC malignant tumour (the CTMCM Homogeneity). Concerning the classical textural features, we notice the importance of the textural features derived from the second and third order EOCM (energy, entropy, correlation, contrast and variance), from the GLCM of order two, three, five and seven and also of the Shannon entropy computed after applying the Wavelet transform, at multiple resolutions. All these features confirm the echogenicity increase in the cases of HCC, as well as the complex and chaotic structure of this malignant tumour.

- **The relevant textural features derived from the edge based CTMCM matrix**

The set of the relevant textural features obtained in this situation is depicted in (8).

{EOCM3_Energy, EOCM3_Variance, Wavelet_Entropy1, GLCM5_Entropy, GLCM7_Energy, Edge_CTMCM_MaxArea, Edge_CTMCM_Entropy, GLCM3_Energy, Wavelet_Entropy4, EOCM3_Contrast, GLCM7_Entropy, Wavelet_Entropy6_ll, Wavelet_Entropy6_hh, Wavelet_Entropy6_hl, Wavelet_Entropy6_lh, Wavelet_Entropy5_lh, Wavelet_Entropy5_ll, Wavelet_Entropy5_hh, Wavelet_Entropy1, EOCM3_Correlation, EOCM_Entropy, EOCM3_Entropy, Wavelet_Entropy2, GLCM7_Correlation, Min_Grey_Level, Wavelet_Entropy4, GLCM_Variance, Wavelet_Entropy3, EOCM3_Homogeneity, GLCM_Contrast, Edge_CTMCM_Correlation, Edge_CTMCM_Contrast}

(8)

We notice that the Maximum Area and the Entropy derived from the second order CTMCM matrix are situated on the top of the corresponding ranking, while the CTMCM Correlation and Contrast are also present in the relevant feature set. Thus, the chaotic structure (CTMCM Entropy), respectively the structural complexity (CTMCM Maximum Area and Contrast) of HCC, as well as the differences in granularity between HCC and the cirrhotic parenchyma on which HCC had evolved, are emphasized in this case, as well. Concerning the old textural features, we remark the minimum grey level, expressing the hyperechogenic nature of the HCC tissue in most of the cases; the Energy

computed based on the third and seventh order GLCM, respectively the Entropy derived from the fifth order GLCM, expressing the differences in echogenicity between HCC and the surrounding cirrhotic parenchyma, respectively the chaotic structure of the malignant tumour; the variance derived from the second and seventh order GLCM characterizing the complexity of the HCC tissue, the correlation derived from the seventh order GLCM standing for the differences in granularity between HCC and the neighbouring cirrhotic parenchyma. The features derived from the third order EOCM matrix and the Shannon entropy computed after applying the Wavelet transform at multiple resolutions are also met at a great extent within the relevant feature set, denoting the complex, chaotic structure of the malignant tumour, in comparison with the cirrhotic parenchyma on which this tumour had evolved.

- **Class differentiation accuracy due to the CTMCM matrices**

Figure 3 depicts the comparison of the classification accuracies obtained for each considered classifier for the same types of feature sets as in the case of the cirrhosis and cirrhotic parenchyma comparison. We can notice that the classification accuracy is always better for the feature sets containing the newly defined textural features than in the case of the old textural feature set. The best classification accuracy, of 84.09% was obtained in the case of the AdaBoost metaclassifier combined with the J48 method for the set of the old textural features combined with the Laws' based CTMCM features. Concerning the arithmetic mean value for all the considered classifiers, the highest value, 79.68%, resulted in the case of the old textural features combined with the edge based CTMCM features, followed by the value of 79.25% obtained in the case of the combination between the old textural features and the Laws' based CTMCM features, respectively by the value of 77.72% resulted in the case when only the old textural features were considered. The MLP classifier provided the best result when the corresponding architecture had one single hidden layer, in all the cases. Regarding the other classification performance parameters, the highest specificity (TN Rate) of 82.7% and the highest AUC of 87.3%, resulted in the case of the adaboost meta-classifier combined with J48, while the highest sensitivity (TP Rate) of 82.7% resulted in the case of the RF classifier.

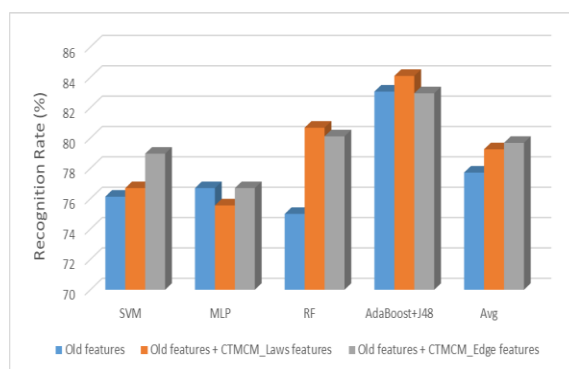


Figure 3: The increase in accuracy due to the newly defined textural features when differentiating between HCC and the cirrhotic parenchyma on which HCC had evolved.

4.3 The Role of the CTMCM Matrices Concerning the Differentiation between HCC and Hemangioma

- **The relevant textural features derived from the Laws' based CTMCM matrix**

The set of the relevant textural features resulted in this case is illustrated in (9):

$$\{ \text{Laws_CTMCM_Homogeneity, Laws_CTMCM_Correlation, GLCM7_Entropy, GLCM5_Contrast, Laws_CTMCM3_Energy, Laws_CTMCM3_Contrast, Directional_Gradient_Variability, GLCM5_Entropy, GLCM3_Energy, GLCM3_Homogeneity, Wavelet_Entropy5_hl, Wavelet_Entropy6_hh, Wavelet_entropy6_hl, GLCM_Homogeneity, Wavelet_Entropy7_hl, GLCM5_Homogeneity} \} \quad (9)$$

The CTMCM Homogeneity and the CTMCM Correlation are in the top of the relevant feature ranking. They emphasize differences in homogeneity (CTMCM Homogeneity) and in granularity (CTMCM Correlation) between the malignant and the benign tumour. The third order CTMCM Energy and third order CTMCM Contrast are also important, standing for the differences in homogeneity, echogenicity (third order CTMCM Energy) and tissue structure complexity (third order CTMCM Contrast) between HCC and hemangioma. Among the relevant textural features obtained in this case we can also notice the features computed based on the second and superior order GLCM, the

directional gradient variability and the entropy computed after applying the Wavelet transform at the second level, on the third (high-low) and fourth (high-high) components, containing the horizontal, respectively the diagonal edges. All these features denote the heterogeneous, chaotic, complex structure of HCC, compared with the more homogeneous structure of the benign tumour.

- **The relevant textural features derived from the edge based CTMCM matrix**

The set of the relevant textural features resulted in this situation is provided in (10):

$$\{ \text{EOCM3_Energy, GLCM7_Entropy, EOCM3_Entropy, GLCM7_Energy, GLCM3_Entropy, Edge_orientation_Variability, Directional_Gradient_Variability, GLCM5_Energy, GLCM3_Homogeneity, Edge_CTMCM_MaxArea, Edge_CTMCM3_Contrast, GLCM_Homogeneity, Wavelet_Entropy7_hl, GLCM5_Homogeneity, GLCM7_Variance, Wavelet_Entropy3, GLCM5_Contrast, Edge_CTMCM3_Correlation, Directional_Gradient_Variance, GLCM_Entropy, Laws_Ripple_Mean, Edge_CTMCM_Contrast, Autocorrelation_Index, Mean_Gray_Level} \} \quad (10)$$

We can notice, from (10), that the CTMCM features are present within the set of the relevant textural features in this case (the CTMCM Maximum Area, the third order CTMCM Contrast, respectively the second order CTMCM Contrast). These features denote differences in structural complexity between HCC and the hemangioma benign tumor. The other features which are among the most relevant textural parameters in this case are those derived from the GLCM matrix of second and superior order, which occupy a large portion of the diagram, some features computed from the EOCM matrix of order three (the Energy and Entropy), the edge orientation variability, the autocorrelation index, the mean grey level, the arithmetic mean of the pixels values after applying the Laws' convolution filter for ripple detection, respectively the entropy computed on both first and second levels after applying the Wavelet transform twice. All these features confirm the chaotic, inhomogeneous, complex character of the malignant tumor tissue.

The specific values of the edge based CTMCM maximum area parameter, for each class (HCC and hemangioma), obtained after applying the technique

of Bayesian Belief Networks in Weka 3.6, are depicted within Table 1. It results that the distribution of the values of the edge based textural microstructures is more balanced in the case of hemangioma, while in the case of HCC, these values are probably grouped towards higher values, as it is assumed that the edges are more emphasized in this case, due to the more complex structure of the malignant tumor.

Table 1: The probability distribution table for the CTMCM Maximum Area.

	$(-\infty, 64658.5]$	$(64658.5, \infty)$
Hemangioma	0.38	0.62
HCC	0.77	0.22

- **Class differentiation accuracy due to the CTMCM matrices**

Figure 4 illustrates the comparison of the classification accuracies obtained when considering the feature sets mentioned before. We can notice a classification accuracy increase in all cases, due to the newly defined textural features. The best classification accuracy, of 88.41%, resulted in the case of the AdaBoost meta-classifier combined with the J48 classifier, corresponding to the feature set containing the old textural features and the Laws' based CTMCM features. In the case of the arithmetic mean (average) of the recognition rates, the most increased value (84.32%) resulted for the feature set that contained the Laws' based CTMCM features, followed by the value of 83.76% obtained in the case when taking into account the edge based CTMCM features, then by the value of 82.005% resulted when taking into account only the old textural feature set. Concerning the MLP classifier, it provided the best results when a one layer architecture was adopted, for the feature set containing only the old features, as well as for the feature set containing the old textural features and the edge based CTMCM features, respectively, when a two layers architecture was adopted, for the feature set containing the old textural features and the Laws' based CTMCM features. The other classification performance parameters resulted as follows: the highest sensitivity (TP Rate), of 84.9% was obtained in the case of the AdaBoost meta-classifier combined with the J48 method; the highest sensitivity (TN Rate) of 88.6% was obtained in the case of SMO; the highest AUC of 89.9%, resulted in the case of MLP.

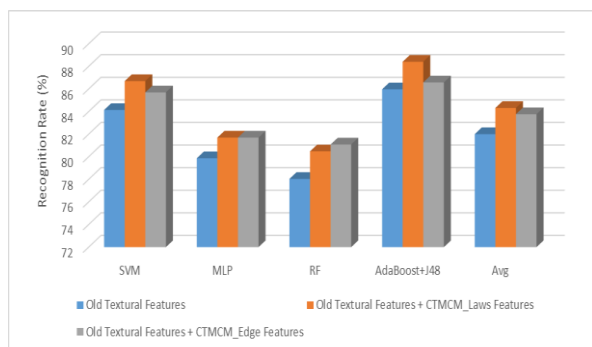


Figure 4: The increase in accuracy due to the newly defined textural features when differentiating between HCC and Hemangioma.

4.4 Discussions

The newly defined CTMCM textural features always resulted among the most relevant textural features in our experiments, being part of the imagistic textural model in the considered cases. These relevant textural features highlighted the increase of the echogenicity, heterogeneity, chaotic structure and structural complexity of the tissue during the restructuring process, from cirrhosis to HCC and also the differences between the malignant and the benign tumoral tissue (HCC versus hemangioma). Another aspect to be noticed is that the features referring to the skewness and kurtosis derived from the superior order histograms (the CTMCM Cluster Shade and the CTMCM Cluster Prominece), respectively the maximum intersection area with a horizontal plane, usually occupied a place in the top of the relevant feature ranking, highlighting, once again, the complex structure of the malignant tumour. We can notice that the edge based CTMCM textural features led to a better classification performance than the Laws' based CTMCM textural features, when differentiating between cirrhosis and cirrhotic parenchyma on which HCC had evolved, respectively between cirrhotic parenchyma and HCC. It results the importance of the edges concerning the refined differentiation between the different phases of liver parenchyma restructuring. In the case of differentiation between HCC and hemangioma, the Laws' based CTMCM textural features overpassed the edge based CTMCM textural feature from classification performance point of view. Thus, in this case, the Laws' based textural microstructures better emphasized the differences between the malignant and benign liver tumours. The best obtained classification performance was above 88% in the case of the differentiation between the malignant and the benign

liver tumours, respectively above 84% when differentiating between HCC and the cirrhotic parenchyma. The classifier that provided the best classification accuracy was AdaBoost combined with the J48 technique, this combination scheme being well known for its performance.

- **Comparison with the state of the art results**

The classification accuracy due to the newly defined textural features, in combination with the formerly existing textural features always overpassed the classification accuracy which was due only to the formerly existing textural features, as shown in the experiments above. Also, this accuracy is comparable with that of the state of the art algorithms, in the case of the differentiation between malignant and benign liver tumors: 88.41% in the case when the CTMCM matrices were employed; above 80% when using classical textural features and classifiers (Sujana et al., 1996); about 90% when using hierarchical wavelet-based features (Yoshida et al., 2003). In the case when distinguishing between the malignant liver tumours and the cirrhotic parenchyma, a recognition rate of 84.09% was obtained when employing the CTMCM matrices within B-mode ultrasound images (in our case), while in the case of employing textural features derived from CEUS images, in combination with classifiers, an accuracy of 90% resulted (Duda et al., 2013). As it can be noticed, the accuracy is lower in the case of differentiation between HCC and the cirrhotic parenchyma, due to the fact that, especially during the intermediate evolution phases, HCC resembles sometimes the surrounding cirrhotic parenchyma. Thus, our solution can be further improved by using more advanced multi-resolution techniques, as well as CEUS images, and also by explicitly taking into account different HCC evolution phases.

5 CONCLUSIONS

The CTMCM matrices demonstrated an obvious contribution concerning the increase of the classification performance and diagnosis accuracy in the case of the HCC malignant tumour and of the pathological phases that precede this form of liver cancer (cirrhosis). The corresponding features were always among the most relevant textural features, considerably improving the imagistic textural model of the considered pathologies. At the end, the resulted classification accuracy was above 84%, in

all cases. In our future research, we aim to further increase the HCC automatic diagnosis accuracy by employing the multi-resolution versions of the CTMCM matrices and of the corresponding Haralick features. We will also consider larger datasets in order to improve the validation procedure and deep learning methods in order to increase the classification performance. We take into account the possibility of using other types of ultrasound images, as well, such as contrast enhanced ultrasound images (CEUS), respectively elastographic images.

REFERENCES

- American liver foundation, 2015. Online: <http://www.liverfoundation.org/abouttheliver/info/>
- Sherman, M. 2005. Approaches to the Diagnosis of Hepatocellular Carcinoma. In *Current Gastroenterology Reports*, vol. 7, no. 1, pp.11-18.
- Sujana, H., Swarnamani, S., 1996. Application of Artificial Neural Networks for the classification of liver lesions by texture parameters. In *Ultrasound in Medicine & Biology*, vol. 22, no. 9, pp.1177 –1181.
- Yoshida, H., Casalino, D., 2003. Wavelet packet based texture analysis for differentiation between benign and malignant liver tumors in ultrasound images. In *Physics in Medicine & Biology*, vol. 48, pp. 3735-3753.
- Madabhushi, A., 2005. Automated Detection of Prostatic Adenocarcinoma from High-Resolution Ex Vivo MRI. In *IEEE Transactions on Medical Imaging*, pp.1611-1626.
- Chikui, T., 2005. Sonographic texture characterization of salivary gland tumors by fractal analysis, In *Ultrasound in Medicine & Biology*, vol. 31, no. 10, pp.1297- 1304.
- Duda, D., Kretowski, M., 2013. Computer-Aided Diagnosis of Liver Tumors Based on Multi-Image Texture Analysis of Contrast-Enhanced CT. Selection of the Most Appropriate Texture Features. In *Studies in Logic, Grammar and Rhetoric*, vol. 35, no. 1, pp. 49–70.
- Khuzir, A., Besar, R., 2009. Identification of masses in digital mammogram using gray level co-occurrence matrices. In *Biomedical Imaging Intervention Journal*, vol. 5, no. 3, pp. e17-e30.
- Masood, K., 2006. Co-occurrence and morphological analysis for colon tissue biopsy classification. In Proceedings of the 4th International Workshop on Information Technology, 2006, Pakistan, pp. 211-216.
- Meyer-Base, A., 2009. *Pattern recognition for medical imaging*, Elsevier, San Diego, California.
- Mitreă, D., Mitreă, P., Nedevschi, S., Lupsor, M., Socăciu, M., Golea, A., Hagi, C., Ciobanu, L., 2012. Abdominal tumor characterization and recognition using superior order co-occurrence matrices, based on ultrasound images. In *Computational and Mathematical Methods in Medicine*, 17 pages.
- Mitreă, D., Nedevschi, S., Socăciu, M., Badea, R., 2012. The Role of the Superior Order GLCM in the Characterization and Recognition of the Liver Tumors from Ultrasound Images. In *Radioengineering*, vol. 21, no. 1, pp. 79-85.
- Mitreă, D., Nedevschi, S., Badea, R., 2014. The Role of the Textural Microstructure Co-occurrence Matrices in the Classification of the Abdominal Tumors. The 10th IEEE ICCP 2014 Conference, Technical University of Cluj-Napoca , pp. 187-190.
- Mitreă, D., Nedevschi, S., Abrudean, M., Badea, R., 2015. Colorectal cancer recognition from ultrasound images, using complex textural microstructure co-occurrence matrices, based on Laws' features, In proceedings of the 38th IEEE International Conference on Telecommunications and Signal Processing, 2015 (TSP 2015), Praga, pp. 458-462.
- Mitreă, D., Nedevschi, S., Badea, R., 2016. The Role of the Complex Extended Textural Microstructure Co-occurrence Matrix in the Unsupervised Detection of the HCC Evolution Phases, based on Ultrasound Images. In Proceedings of International Conference on Pattern Recognition Applications and Methods (ICPRAM 2016), Roma, pp. 698-705.
- Davis, L.S., Clearman, M., Aggarwal, J., 1979. A Comparative Texture Classification Study Based on Generalized Cooccurrence Matrix. Proceedings of the 18-th IEEE Conference on Decision and Control, pp. 71-78.
- Sujatha, B., Kumar, V., Harini, P., 2012. A new logical compact LBP Co-Occurrence Matrix for Texture Analysis. In *International Journal of Scientific & Engineering Research*, vol. 3, no. 2, pp. 1-5, 2012.
- Sujatha, B., Sekhar Reddi, C., 2013. Texture classification using texton co-occurrence matrix derived from texture orientation. In *International J. Soft Computing and Eng*, vol. 2, no. 6, pp. 18-23.
- Laws, K.I., 1980. Rapid texture identification. In *SPIE Vol. 238 Image Processing for Missile Guidance*, pp.76-380.
- Nanni, L., Brahnam, S., Ghidoni, S., Menegatti, E., Barrier, T., 2013. "Different Approaches for Extracting Information from the Co-Occurrence Matrix". In *PloS One Journal*, Vol.8, No. 12, 2013, pp. 1-9.
- Kirsch, R., 1971. Computer determination of the constituent structure of biological images. In *Computers and Biomedical Research*, Vol.4, No.3, pp. 315–328.
- Hall, M., 2003. Benchmarking attribute selection techniques for discrete class data mining. In *IEEE Trans On Knowledge and Data Eng.*, vol. 15, no. 3, pp. 1-16.
- Weka3, Data Mining Software in Java, 2017. Online: <http://www.cs.waikato.ac.nz/ml/weka>.
- Duda, R., 2003 *Pattern Classification*, Wiley Interscience, Hoboken, New Jersey.